

Simplification, Expansion and Enhancement of Direct Interior Point Algorithm for Power System Maximum Loadability

Youjie Dai, *Student Member, IEEE*, James D. McCalley, *Senior Member, IEEE*, and Vijay Vittal, *Fellow, IEEE*

Abstract—Power system maximum loadability is a crucial index. The direct interior point algorithm was introduced by several researchers to calculate power system maximum loadability. This paper simplifies the direct interior point model and applies it to various optimization problems. Zone-based maximum loadability problems are discussed. Weight factors and tie line flows are included. ATC (Available Transfer Capability) calculation is also investigated. The meaning and applications of “shadow price” are explained and shown. The principle of oscillation for this algorithm is explained. The factors that influence the algorithm’s speed and convergence are investigated. Our research proves the interior point algorithm is a powerful tool that can handle various kinds of maximum loadability problems.

Index Terms—Interior point, maximum loadability.

I. INTRODUCTION

POWER system loadability calculation is a traditional problem which has received more attention recently due to power industry restructuring. The research on this problem moves along two different directions. The first direction, represented by reference [1] and other work, calculates voltage stability indices by assuming some mode of generation allocation and tracing the load increment. The continuation power flow is one of the most promising approaches in this direction. Algorithms to calculate the nearest bifurcation point from an interior or an exterior point of the feasible region have been shown in references [2], [3], and many other papers respectively. The second direction, as in [4] and [5], emphasizes the optimal adjustment of generation and load under constraints, and regards the problem as an optimal power flow problem. Linear programming [3], or sequential linear programming [5] is normally used to solve the optimization problem. The power flow equations are largely simplified, which makes it hard to trace the voltage stability saddle node. Recently, the two directions were merged in [6]–[9], under the unified direct interior point algorithm. These works provided insight into the potential application of the interior point algorithm in this area.

The interior point algorithm is not new. It was first developed by Frisch [10] in 1955. However, the milestone should be attributed to Karmarkar [11], who proved and showed the interior point algorithm he developed is much faster than the traditional

simplex method for large linear programming problems. This immediately launched a research campaign on interior point algorithms which is still going on today. In 1992, Mehrotra’s predictor-corrector interior point method [12] was regarded as an important improvement. Most recent developments on interior point algorithms can be found in [13], [14].

Interior point algorithms have been used for optimal power flow [15], voltage stability analysis [8], unit commitment calculation [16], and many other optimization problems in power systems. For system maximum loadability and minimum load curtailment problems, references [6]–[9] propose different direct interior point algorithms respectively. However, according to our observation, the first order Kuhn–Tucker (KT) equations can be largely simplified. Therefore, in this paper, a simplified model derived from the first order KT conditions is proposed, which reduces the problem size to be about one fourth of the original one. We further investigate the influence of various factors on the performance of our algorithm, and we propose some techniques to improve its efficiency in this paper.

We also expand our model to calculate maximum loadability and minimum load curtailment when zone-based constraints are imposed on the loads. This formulation enables calculation of available transfer capability (ATC) from one generation company to a customer. Finally, the meaning of “shadow price” in our model is explained and utilized to identify the most effective means of increasing the maximum loadability. Our model is applied to IEEE RTS 96 system for various kinds of maximum loadability (ML) analysis.

II. MATHEMATICAL MODELS FOR MAXIMUM LOADABILITY PROBLEMS

We encountered a maximum loadability (ML) problem when we performed planning stage risk assessment. Our question is, how to estimate risk due to load curtailment hour by hour during a whole year? If we can identify the maximum loadability of a power system, the risk can be estimated easily by comparing real load with the maximum loadability. This idea was first proposed by [6] and [7] for voltage stability reliability evaluation. Since the whole system is regarded as one zone, we call it one zone model. However, the strong assumption of one zone model makes it impractical in most power systems. Therefore, we have developed multi-zone model to make the ML problem more general. Furthermore, we found it easy for us to expand our ML model to ATC calculation. We describe these ML models in the following subsections.

Manuscript received February 14, 2000. This work was supported by the National Science Foundation Grant ELS9502790 and the Electric Power Research Institute, Contract W08604-01.

The authors are with Iowa State University (e-mail: {ydai;jdm}@iastate.edu; vittal@vulean.ee.iastate.edu).

Publisher Item Identifier S 0885-8950(00)07737-3.

A. One Zone Model

Because identification of maximum loadability requires variation in load, one must make an assumption regarding how individual loads vary with respect to each other. The simplest assumption is that all loads vary proportionally. So the whole system is considered as a big zone. The maximum loadability problem can then be modeled as follows.

$$\max g(P_{D\Sigma}) \quad (1)$$

where $g(P_{D\Sigma}) \triangleq P_{D\Sigma} = \sum_{k=1}^N P_{Dk}$, subject to

$$P_{gk} - p_{dk}P_{D\Sigma} - P_{ek} = 0, \quad k = 1, \dots, N \quad (2)$$

$$Q_{gk} - q_{dk}P_{D\Sigma} - Q_{ek} = 0, \quad k = 1, \dots, N \quad (3)$$

$$P_{gk} \min \leq P_{gk} \leq P_{gk} \max, \quad k \in \Omega_p \quad (4)$$

$$Q_{gk} \min \leq Q_{gk} \leq Q_{gk} \max, \quad k \in \Omega_q \quad (5)$$

$$V_k \min \leq V_k \leq V_k \max, \quad k \in \Omega_v \quad (6)$$

where

$g(P_{D\Sigma})$ is the objective function of loads. In this case, it is the total summation of loads, which is also represented by $P_{D\Sigma}$.

P_{gk} is the active generation power at bus k .

Q_{gk} is the reactive generation power at bus k .

p_{dk} is the ratio constant for $P_{Dk}/P_{D\Sigma}$, where P_{Dk} is the active load at bus k . We always have

$$\sum_{k=1}^N p_{dk} = 1 \quad (7)$$

q_{dk} is the ratio constant for $Q_{Dk}/P_{D\Sigma}$, where Q_{Dk} is the reactive load at bus k .

$P_{gk} \min, P_{gk} \max, Q_{gk} \min, Q_{gk} \max, V_k \min, V_k \max$ are lower and upper bounds for P_{gk}, Q_{gk} and V_k respectively.

Ω_p is a set of buses which has P_g as a variable. We do not use the generation bus set because when $P_{gk} \min = P_{gk} = P_{gk} \max$, P_{gk} becomes a constant rather than a variable, bus k is then excluded from Ω_p .

Ω_q is a set of buses which has Q_g as a variable.

Ω_v is a set of buses which has V as a variable.

N is the number of buses.

The terms P_{ek} and Q_{ek} in equations (2) and (3) are computed using the power flow-equations, i.e.,

$$P_{ek} = V_k \sum_{l=1}^N Y_{kl} V_l \cos(\theta_k - \theta_l - \phi_{kl}) \quad (8)$$

$$Q_{ek} = V_k \sum_{l=1}^N Y_{kl} V_l \sin(\theta_k - \theta_l - \phi_{kl}) \quad (9)$$

where Y is the admittance matrix of the network, θ is the bus voltage angle, $\phi_{kl} = \angle Y_{kl}$.

B. Multi-Zone Model

The assumption that all loads vary proportionally is not appropriate when load curtailment is considered. For example, when a bus load is limited by voltage security problems, the loads of other buses should not be necessarily curtailed to alleviate this problem. Fortunately, most power systems can be

divided into different zones, so that it is reasonable for us to assume all loads change proportionally in each zone. Under the slightly changed assumption, by further taking into account the constant part in loads (which can be a constant tie line flow support to or from some other area), we can rewrite equations (2) and (3) as follows.

$$\begin{aligned} P_{gk} - P_{Dk}^0 - p_{dk}P_{D\Sigma i} - P_{ek} &= 0, & k \in D_i, \\ Q_{gk} - Q_{Dk}^0 - q_{dk}P_{D\Sigma i} - Q_{ek} &= 0, & k \in D_i, \end{aligned} \quad (10)$$

$$i = 1, \dots, d \quad (11)$$

where $P_{D\Sigma} = (P_{D\Sigma 1}, \dots, P_{D\Sigma d})^T$ is the total load vector for zones, P_{Dk}^0 and Q_{Dk}^0 are the constant active and reactive parts of the load at bus k .

The loads of different zones can have different balance priority, as indicated by the prices they pay. This can be accommodated by applying different weighting factors for different zones. Then the objective function for the ML problem becomes

$$g(P_{D\Sigma}) = \sum_{i=1}^d w_i P_{D\Sigma i} \quad (12)$$

where w_i is the weighting factor for zone i .

When upper and lower bounds are applied to $P_{D\Sigma i}$ such that

$$0 \leq P_{D\Sigma i} \leq P_{D\Sigma i} \max \quad (13)$$

then the problem becomes the minimum load curtailment problem, i.e., for the given load level, we want to calculate the minimum load required curtailed to meet all constraints.

C. Available Transfer Capability

If we only free the generation of a source bus and the load of a sink bus, and fix the generation and load of all other buses, we can calculate the ATC (available transfer capability). However, if we want to include the thermal overload constraint on each line, we should let $i_l \leq I_l$, where i_l is the current (in absolute value) through line l , and I_l is line l 's thermal overload current rating. u_l can be expressed as follows.

$$\begin{aligned} i_l &= y_l \Delta V_l \\ &= \sqrt{(g_l^2 + b_l^2) (V_i^2 + V_j^2 - 2V_i V_j \cos(\theta_i - \theta_j))} \end{aligned} \quad (14)$$

where y_l is the admittance (in absolute value) of line l , g_l and b_l are the conductance and susceptance of line l . If we denote

$$f_l = V_i^2 + V_j^2 - 2V_i V_j \cos(\theta_i - \theta_j) \quad (15)$$

we can translate the thermal overload constraints into the following form.

$$0 \leq f_l \leq \frac{I_l^2}{g_l^2 + b_l^2}, \quad l = 1, \dots, L \quad (16)$$

Here L is the number of lines, and l_i and l_j are the bus numbers of line l 's two buses,

III. GENERALIZED INTERIOR POINT ALGORITHM CALCULATION MODEL

From the previous section, the generalized maximum loadability problem can be expressed as follows.

$$\min g(P_{D\Sigma}(z, y)) \quad (17)$$

subject to

$$h(x, y) = 0 \quad (18)$$

$$F_l \leq F(z, y) \leq F_u \quad (19)$$

$$z_l \leq z \leq z_u \quad (20)$$

We solve the following alternative problem in the interior point algorithm [7], [9]

$$\begin{aligned} \min g(z, y) - \mu \sum_j \ln r_{lj} - \mu \sum_j \ln r_{uj} \\ - \mu \sum_j \ln s_{lj} - \mu \sum_j \ln s_{uj} \end{aligned} \quad (21)$$

subject to

$$h(z, y) = 0 \quad (22)$$

$$F(z, y) - r = 0 \quad (23)$$

$$r - r_l - F_l = 0 \quad (24)$$

$$r + r_u - F_u = 0 \quad (25)$$

$$z - s_l - z_l = 0 \quad (26)$$

$$z + s_u - z_u = 0 \quad (27)$$

The Lagrange function for this problem is as follows.

$$\begin{aligned} L = g(z, y) - \mu \sum_j \ln r_{lj} - \mu \sum_j \ln r_{uj} - \mu \sum_j \ln s_{lj} \\ - \mu \sum_j \ln s_{uj} - \lambda_h^T h(z, y) - \lambda_f^T (F(z, y) - r) \\ - \pi_{rl}^T (r - r_l - F_l) - \pi_{ru}^T (r + r_u - F_u) \\ - \pi_{zl}^T (z - s_l - z_l) - \pi_{zu}^T (z + s_u - z_u) \end{aligned} \quad (28)$$

The KT first order optimality condition gives the following equations.

$$\nabla_z L = \nabla_z g - J_{hz}^T \lambda_h - J_{fz}^T \lambda_f - \pi_{zl} - \pi_{zu} = 0 \quad (29)$$

$$\nabla_r L = \lambda_f - \pi_{rl} - \pi_{ru} = 0 \quad (30)$$

$$\nabla_y L = \nabla_y g - J_{hy}^T \lambda_h - J_{fy}^T \lambda_f = 0 \quad (31)$$

$$\nabla_{r_l} L = -\mu R_l^{-1} e + \pi_{rl} = 0 \quad (32)$$

$$\nabla_{r_u} L = -\mu R_u^{-1} e - \pi_{ru} = 0 \quad (33)$$

$$\nabla_{s_l} L = -\mu S_l^{-1} e + \pi_{zl} = 0 \quad (34)$$

$$\nabla_{s_u} L = -\mu S_u^{-1} e - \pi_{zu} = 0 \quad (35)$$

$$\nabla_{\pi_{rl}} L = -(r - r_l - F_l) = 0 \quad (36)$$

$$\nabla_{\pi_{ru}} L = -(r + r_u - F_u) = 0 \quad (37)$$

$$\nabla_{\pi_{zl}} L = -(z - s_l - z_l) = 0 \quad (38)$$

$$\nabla_{\pi_{zu}} L = -(z + s_u - z_u) = 0 \quad (39)$$

$$\nabla_{\lambda_h} L = -h(z, y) = 0 \quad (40)$$

$$\nabla_{\lambda_f} L = -(F(z, y) - r) = 0 \quad (41)$$

where $J_{hz} = (\partial h / \partial z)$, $J_{fz} = (\partial F / \partial z)$, $J_{hy} = (\partial h / \partial y)$, $J_{fy} = (\partial F / \partial y)$, $e = [1, 1, \dots, 1]^T$, $S_l \triangleq \text{diag}(s_{l1}, \dots, s_{lm})$, $S_u \triangleq \text{diag}(s_{u1}, \dots, s_{um})$, $R_l \triangleq \text{diag}(r_{l1}, \dots, r_{lm})$, $R_u \triangleq \text{diag}(r_{u1}, \dots, r_{un})$

Until this step, we have followed the same steps as described in [7] and [9]. However, [7] and [9] solve eqs. (29)–(41) directly using a Newton–Raphson method, which requires 16N equations. By direct observation, it is possible for us to eliminate some variables by simple transformations. Denote $\pi_z = \pi_{zl} + \pi_{zu}$, $\pi_r = \pi_{rl} + \pi_{ru}$, and from equation (30), we can eliminate λ_f . From equations (32)–(35) we can eliminate π_z

and π_r . From equations (36)–(39) we can eliminate slack variables r_l, r_u, s_l, s_u . After these modifications, we can rewrite the equations in the following compact form.

$$\nabla_z g - J_{hz}^T \lambda_h - J_{fz}^T \pi_r - \pi_z = 0 \quad (42)$$

$$\nabla_y g - J_{hy}^T \lambda_h - J_{fy}^T \pi_r = 0 \quad (43)$$

$$h(z, y) = 0 \quad (44)$$

$$F(z, y) - r = 0 \quad (45)$$

where

$$\begin{cases} \pi_{ri} = \mu \left(\frac{1}{r_i - F_{il}} - \frac{1}{F_{iu} - r_i} \right), & i = 1, \dots, n \\ \pi_{zi} = \mu \left(\frac{1}{z_i - z_{il}} - \frac{1}{z_{iu} - z_i} \right), & i = 1, \dots, m \end{cases} \quad (46)$$

Now we only need to solve about $4N$ equations at the worst case, almost one-fourth of the original KT first order equations. It is also just about twice the number of power flow equations. Although this simplification may degrade the sparsity of the original KT first order equations, our equations are much simpler in form, and the corresponding Hessian matrix is easier to derive. Further, since our equations are simply transformed from the original equations, the speed of our method for every iteration is at least as fast as that of solving the original equations.

A. Model for Zone-Based Maximum Loadability

For the zone-based ML objective function given by eq. (12), $h(z, y)$ represents the power flow equations given by eqs. (10) and (11). $F(z, y)$ does not exist because thermal overload constraints are not considered in this model. The constrained variable vector z includes P_{gk} when bus $k \in \Omega_p$, Q_{gk} when bus $k \in \Omega_q$, V_k when bus $k \in \Omega_v$. The unconstrained variable vector y includes θ_k for all bus k excluding the slack bus, and $P_{D\Sigma i}$ for all zone i . Invoking this model into the eqs. (42)–(45) we obtain:

$$\sum_{l=1}^N \pi_{pl} \frac{\partial P_{el}}{\partial \theta_k} + \sum_{l=1}^N \pi_{ql} \frac{\partial Q_{el}}{\partial \theta_k} = 0, \quad l \in \Omega_\theta \quad (47)$$

$$\sum_{l=1}^N \pi_{pl} \frac{\partial P_{el}}{\partial V_k} + \sum_{l=1}^N \pi_{ql} \frac{\partial Q_{el}}{\partial V_k} + \pi_{vk} = 0, \quad k \in \Omega_v \quad (48)$$

$$P_{gk} - P_{Dk}^0 - p_{dk} P_{D\Sigma i} - P_{ek} = 0, \quad k = 1, \dots, N \quad (49)$$

$$Q_{gk} - Q_{Dk}^0 - q_{dk} P_{D\Sigma i} - Q_{ek} = 0, \quad k = 1, \dots, N \quad (50)$$

$$w_i + \sum_{k \in D_i} \pi_{pk} p_{dk} + \sum_{k \in D_i} \pi_{qk} q_{dk} = 0, \quad i = 1, \dots, d \quad (51)$$

where

$$\pi_{pl} = \begin{cases} \mu \left(\frac{1}{P_{gl} - P_{gl \min}} - \frac{1}{P_{gl \max} - P_{gl}} \right), & l \in \Omega_p \\ a \text{ variable}, & l \notin \Omega_p \end{cases} \quad (52)$$

$$\pi_{ql} = \begin{cases} \mu \left(\frac{1}{Q_{gl} - Q_{gl \min}} - \frac{1}{Q_{gl \max} - Q_{gl}} \right), & l \in \Omega_q \\ a \text{ variable}, & l \notin \Omega_q \end{cases} \quad (53)$$

$$\pi_{vl} = \mu \left(\frac{1}{V_l - V_{l \min}} - \frac{1}{V_{l \max} - V_l} \right), \quad l \in \Omega_v \quad (54)$$

B. Model for Zone-Based Minimum Load Curtailment

When the minimum load curtailment problem is considered, $P_{D\Sigma i}$ becomes a constrained variable for every zone i . As a result, eq. (51) becomes:

$$w_i + \sum_{k \in D_i} \pi_{pk} P_{dk} + \sum_{k \in D_i} \pi_{qk} Q_{dk} + \pi_{Di} = 0 \quad (55)$$

where

$$\pi_{Di} = \mu \left(\frac{1}{P_{D\Sigma i}} - \frac{1}{P_{D\Sigma i \max} - P_{D\Sigma i}} \right) \quad (56)$$

C. Model for ATC Calculation

In the ATC calculation, when thermal overload constraints are taken into account, the term $F(z, y)$ should be included in eqs. (42)–(45). As a result, eqs. (51) and (52) become:

$$\sum_{l=1}^N \pi_{pl} \frac{\partial P_{el}}{\partial \theta_k} + \sum_{l=1}^N \pi_{ql} \frac{\partial Q_{el}}{\partial \theta_k} + \sum_{l=1}^L \pi_{rl} \frac{\partial f_l}{\partial \theta_k} = 0, \quad k \in \Omega_\theta \quad (57)$$

$$\sum_{l=1}^N \pi_{pl} \frac{\partial P_{el}}{\partial V_k} + \sum_{l=1}^N \pi_{ql} \frac{\partial Q_{el}}{\partial V_k} + \pi_{vk} + \sum_{l=1}^L \pi_{rl} \frac{\partial f_l}{\partial V_k} = 0, \quad k \in \Omega_v \quad (58)$$

Then we need to add the following equations.

$$f_l - r_l = 0, \quad l = 1, \dots, L \quad (59)$$

where f_l is a function expressed in (15), π_r is calculated by expression (46), and the upper limit $F_{iu} = (I_i^2/g_i^2 + b_i^2)$.

IV. THE SOLUTION ALGORITHM

We use Newton–Raphson method to solve the equations. Denote J_b to be the big Jacobian matrix for the equations (42)–(45), then we have

$$\begin{bmatrix} \Delta z^k \\ \Delta y^k \end{bmatrix} = -J_b^{-1} G(z^k, y^k) \quad (60)$$

at every step, where $G(\cdot, \cdot)$ is the left hand side function vector of the equations. However, we have to keep z^{k+1} within the feasible region. Therefore, for each iteration, we will choose the maximum α such that $z^k + \alpha \Delta z^k \in S$, where S is the feasible region. Once we get α , we choose z^{k+1} to be between z^k and $z^k + \beta \alpha \Delta z^k$, where $\beta = 0.9995$, and choose z^{k+1} such that $\|G(z^{k+1}, y^{k+1})\|_\infty$ is minimized, or at least less than $\|G(z^k, y^k)\|_\infty$. One possible algorithm is as follows.

1. Equally divide z^k and $z^k + \beta \alpha \Delta z^k$ into n_s segments, where n_s is chosen appropriately.
2. At the end of each segment, check $\|G(z, y)\|_\infty$ to find the minimum value and the corresponding point (\bar{z}, \bar{y}) .
3. If $(\bar{z}, \bar{y}) \leq (z^k, y^k)$, we have $\begin{cases} z^{k+1} = \bar{z} \\ y^{k+1} = \bar{y} \end{cases}$ Otherwise find a small enough $\gamma > 0$ such that

$$\begin{cases} z^{k+1} = z^k + \gamma \alpha \Delta z^k \\ y^{k+1} = y^k + \gamma \alpha \Delta y^k \end{cases}$$

and $\|G(z^{k+1}, y^{k+1})\|_\infty \leq \|G(z^k, y^k)\|_\infty$. When J_b is continuous, such a γ always exists.

It has been shown that by making μ small enough, the optimal solution of the interior point optimization problem eqs. (42)–(45) can be arbitrarily near the optimal solution [13]. However, when μ is very small, the Newton–Raphson method does not converge quickly. So we desire to begin the algorithm with a large value of μ , so as to enhance convergence speed, and then decrease it as we near the solution in order to improve solution accuracy. References [6] and [9] suggest a way to make use of π variables and slack variables to adjust μ . However, since now π_{pk} is a function of P_{gk} when $k \in \Omega_p$, and π_{qk} is a function of Q_{gk} when $k \in \Omega_q$, we can not use this suggested strategy. Instead, we use the following algorithm.

1. Pick up a starting value $\mu = \mu_0$, calculate $G_0 = \|G_{\mu_0}(z_0, y_0)\|_\infty$, set $G_1 = G_0$.
2. If after 3 iterations $\|G\|_\infty$ reduces by less than 10%, set $\mu = 10\mu$, and $G_0 = \|G_\mu(z, y)\|_\infty$.
3. If $\|G\|_\infty \leq (1/10)G_1$, or $\|G\|_\infty \leq 0.01$, set $\mu = (1/10)G_1$.
4. If $\|G\|_\infty \leq \varepsilon$ and $\mu \leq \mu_{\min}$, stop, where ε and μ_{\min} are small positive numbers chosen by the user; otherwise go to 2.

V. FACTORS THAT INFLUENCE THE ALGORITHM'S SPEED AND CONVERGENCE

According to our experience, the μ adjustment scheme, the initial point, and the power flow equation multiplier are the three main factors that influence the algorithm's speed and convergence.

Consider a simple interior point problem as follows.

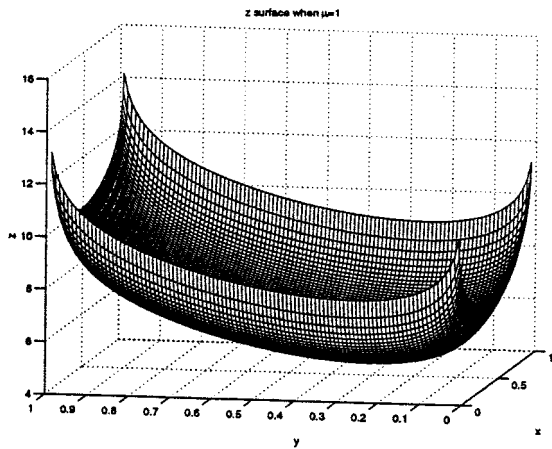
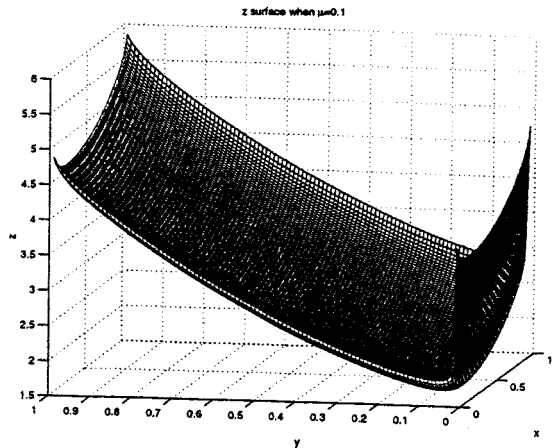
$$\begin{aligned} \min z = & (x+1)^2 + y^2 - \mu \ln(1-x) - \mu \ln x \\ & - \mu \ln(1-y) - \mu \ln y \end{aligned} \quad (61)$$

subject to

$$\begin{aligned} 0 & \leq x \leq 1 \\ 0 & \leq y \leq 1 \end{aligned}$$

A. Oscillations Caused by Small μ

When $\mu = 1$, the z -surface within the feasible region is shown in Fig. 1; when $\mu = 0.1$, the z -surface within the feasible region is shown in Fig. 2. From the two figures, we can see that when μ is large, the z -surface is smooth, therefore we can easily get the optimal solution. When μ is small, the z -surface has a sharp fold near the boundary. When we come to a point just before this trench, from the algorithm point of view, we do not recognize the upcoming boundary wall at this point, and we still head toward the unconstrained optimal solution $(-1, 0)$. In the next iteration, we will encounter the boundary, and we will have to settle on a new point just inside the boundary in order to maintain feasibility. This new point may be between the trench and the boundary, or it may be to the left of the trench. If the point is between the trench and the boundary, then the algorithm will recognize the steep fall of the trench and move into it. On the other hand, if the point is to the left of the trench, it will again move toward the boundary and the process will repeat. Therefore, since the optimum $(0, 0)$ is at the bottom of the trench, the

Fig. 1. z -surface when $\mu = 1$.Fig. 2. z -surface when $\mu = 0.1$.

algorithm is prone to oscillation under this condition, when μ is small.

B. Oscillations Caused by Power Flow Equations

Now let us assume the upper and lower limits on variables constitute a bounded space. Power flow equations constitute a hypercurve. The intersection of the bounded space and the hypercurve is the feasible region. Referring to Fig. 2, when the initial point 1 (IP1) is near the upper bound, it moves toward the unconstrained optimal solution and hits the upper bound. However, if the power flow equations are not satisfied, the point is not on the hyper curve. Therefore the algorithm is prone to oscillation near the boundary in order to move toward the optimal point on the hypercurve. On the other hand, if we start from IP2, which is far away from the boundary, it will recognize the existence of the power flow hypercurve and merge into it somewhere before the boundary. Then it moves along the hypercurve until it hits the boundary. Since the solution now is feasible, further iterations are not needed. The process is shown in Fig. 3.

C. Convergence Enhancements

Choosing the initial point in the interior rather than near the boundary and starting μ with a large value are the measures to

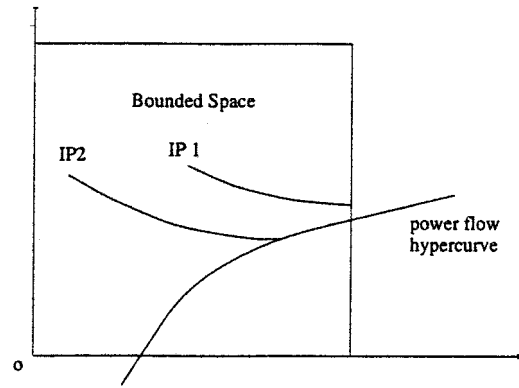


Fig. 3. The influence of initial point position.

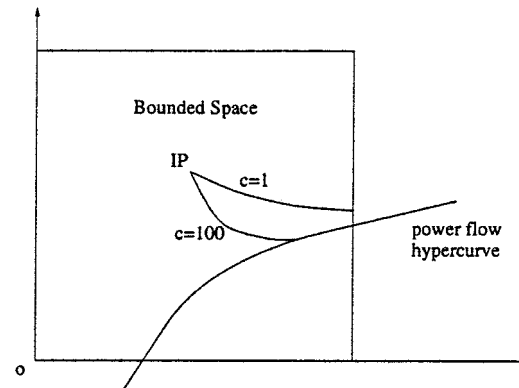


Fig. 4. The influence of power flow multiplier.

avoid oscillation. In our subroutine, μ starts from a large value, gets adjusted to a smaller value after each convergence, and if oscillation is encountered, μ is increased.

Another method is to multiply the power flow equations with a large multiplier c , say, 100. This does not change the solution. However, since we emphasize the importance of power flow equations, we are expected to merge into the hypercurve faster, the number of iterations can then be reduced. The process is as shown in Fig. 4.

VI. NUMERICAL EXAMPLES

A. Voltage Stability Limit Result Compared with VSTAB

VSTAB contains a standard continuation power flow calculation program developed by Powertech Labs Incorporated [17]. We compare results from our software with those from VSTAB in order to provide validation evidence.

Fig. 5 shows the IEEE RTS'96 system. For the typical case given in [18], we choose bus 13 as the swing bus, relieve the generation limits at this bus to be ineffective, and fix all other active generation power. We also choose $V_{\max} = 1.05$ pu, $V_{\min} = 0.90$ pu for all generation buses, and $V_{\max} = 1.15$ pu, $V_{\min} = 0.85$ pu for all load buses. The maximum loadability calculated by our program is 4048 MW, while the VSTAB's calculation result is 4025 MW. The two results coincide with each other very well. This verifies that our program is correct. Furthermore, since VSTAB does not identify the exact bifurcation point, we think our result is more accurate.

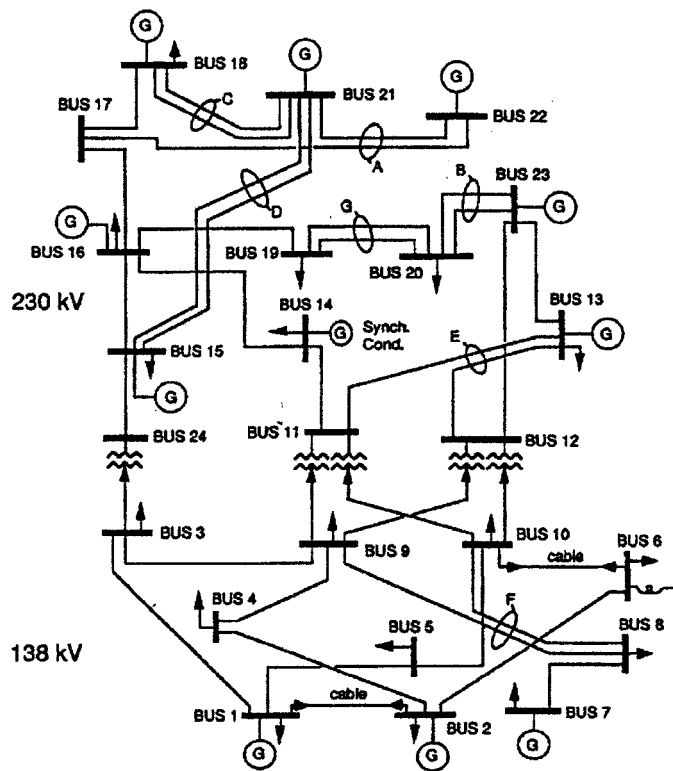


Fig. 5. The IEEE RTS'96 system.

Our approach is very attractive because, for a specified unit commitment, it can also identify the dispatch that maximizes loadability. As an illustration, we repeat the previous calculation with real power injection at each generation bus defined as a decision parameter. This time, the maximum loadability increases to 4208 MW as a result of the optimized dispatch. Furthermore, we can activate the generation limits on the swing bus, which is required for a realistic solution, to identify maximum loadability of 3358 MW. This value is 47 MW less than the installed capacity. This difference is due to losses in the transmission network.

B. Zone-Based Maximum Loadability Calculations

As described in Section II-B, the maximum loadability algorithm may not converge for some particularly stressed scenarios. This occurs, for example, when we utilize the unit commitment pattern of Table I and outage line 6–10.¹ So we turn to the minimum curtailment problem to identify a feasible, maximum loadability under these conditions. In doing so, we define the following zones:

- Zone 1 includes buses 11–24. It is mainly a generation provider.
- Zone 2 includes buses 1–5, 9, 10. It is mainly a load consumer.
- Zone 3 includes buses 7, 8. It is a heavy load center loosely connected with the system.

¹This convergence problem is caused by the loss of a significant reactive resource in the form of the 6–10 line, which is actually a cable. With the shunt reactor still on at bus 6, it is not apt to achieve an acceptable voltage.

TABLE I
UNIT COMMITMENT PATTERN FOR ANALYSIS I (IN MW OR MVAR)

Gen. bus	P_{gmax}	P_{gmin}	Q_{gmax}	Q_{gmin}
14	0	0.00	200	-50
15	155	54.25	80	-50
16	155	54.25	80	-50
18	400	100.00	200	-50
21	400	100.00	200	-50
22	250	0.00	80	-50
23	660	248.50	310	-125

- Zone 4 includes only bus 6. Since the shunt reactor is not cut off after line 6–10's outage, bus 6's load is expected to suffer low voltage.

The maximum generations at this point relates to the choice of weights [see eq. (13)] and the choice of limits on zone load powers [see eq. (14)]. Regarding choice of weights, one approach is to choose them in proportion to the mean energy rates paid by all customers in the zones. This approach would suggest that the zones themselves should be identified according to some maximum variance from the mean. Although the lower limits on zone load powers should be chosen as at least 0, one might also choose them equal to the amount of firm load in the region. The upper limits on zone load powers could be set to some very large values each of which are obviously infeasible. The minimum load curtailment solution would then identify the maximum loadability, assuming generation capacity constraints for each zone (as total generation capacity plus total transmission capability into the zone). Still a third approach would be to use the zone forecasted load increased by four standard deviations. For the system condition described above, we choose $w = [1, 1, 1, 1]$, $P_{D\Sigma \min} = [0, 0, 0, 0]$, $P_{D\Sigma \max} = [957.3, 567.6, 186.7, 85.8]$ MW, where the upper limits represent the zone forecasted load increased by four times the standard deviation. The solution is $P_{D\Sigma} = [957.3, 219.3, 132.9, 0]$ MW, for a total load of 1309.5 MW. If we remove the bus 6 shunt reactor, the solution becomes $P_{D\Sigma} = [957.3, 567.5, 149.6, 42.2]$ MW, for a total load of 1716.6 MW.

C. ATC Calculation

Suppose the system is operating under the conditions described in Section VI-A. Then a new contract requires the generation company who owns bus 13 and bus 23 to provide a new load customer at bus 8. The question is what is the maximum load the system can provide at bus 8. It can be calculated by our ML subroutine by setting variable values as follows.

- 1) The entire system is a single zone.
- 2) P_{Dk}^0 and Q_{Dk}^0 are fixed loads for $k \neq 13$ and $k \neq 23$.
- 3) $p_{dk} = 0$, $q_{dk} = 0$ when $k \neq 13$ and $k \neq 23$.
- 4) P_{gk} , V_{gk} are fixed for generation buses except buses 13 and 23.
- 5) Q_{gk} are allowed to adjust within ranges.

The maximum loadability of bus 8 is 418.6 MW. Subtracting the base case bus 8 loading of 171 MW, the ATC between supply

TABLE II
c VS. NUMBER OF ITERATIONS

Gen. bus	P_{gmax}	P_{gmin}	Q_{gmax}	Q_{gmin}
1	192	62.00	80	-50
2	192	62.00	80	-50
13	591	206.85	240	0
14	0	0.00	200	-50
15	215	66.25	110	-50
16	155	54.25	80	-50
18	400	400.00	200	-50
21	400	400.00	200	-50
22	300	0.00	96	-60
23	660	248.50	310	-125

buses 13 and 23 and demand bus 8 is 247.6 MW. We mention two additional points of interest. First, base case generation levels of $P_{g13} = 186.7$ MW, $P_{g23} = 660$ MW, compared with maximum loadability generation levels of $P_{g13} = 585.7$ MW, $P_{g23} = 541.0$ MW, indicates bus 13 generation power increased by 379 MW but bus 23 generation power decreased by 119 MW, for a net increase of 280 MW. Second, the net generation increase of 280 MW is 32.4 MW more than the increase in bus 8 load of 247.6 MW. This 32.4 MW is used to supply the transmission losses imposed by the increased power transfer.

If we include the continuous thermal rating constraints, the bus 8 maximum loadability becomes 393.6 MW, line 7–8 is constrained. If we use long-term emergency ratings or short-term emergency ratings as thermal overload constraints, the bus 8 maximum loadability is 418.6 MW, and no line is constrained. Therefore, when transmission companies are willing to take thermal overload risk, they can incur greater profit.

D. Power Flow Multiplier's Influence

Table II reports on some experiments run to identify the influence of the multiplier c described in Section V-C. Here, we show the number of the algorithm iterations required for various values of c . It appears that choosing $c = 100$ is appropriate for this particular system.

VII. "SHADOW PRICE" ANALYSIS

A. "Shadow Price" for Variables

"Shadow prices" refer to π_{ri} ($i = 1, \dots, n$) and π_{zj} ($j = 1, \dots, m$) in expression (46). They have specific meaning in optimization theory. According to equation (46), when z_k hits the upper bound, $\pi_{zk} < 0$; when z_k hits the lower bound, $\pi_{zk} > 0$; when z_k is far from both bounds, π_{zk} is very near zero as μ is near zero. On the other hand, according to optimization theory, π_{zk} can be interpreted as the decrement of the objective function due to the per unit decrement of the z_k max when z_k hits the upper bound, or the decrement of the Lagrange function due to the per unit decrement of the z_k min when z_k hits the lower bound. Therefore it reflects the "price" of the binding constraint. When z_k hits the upper bound, as z_k max increases Δz_k , the total load will increase $-\pi_{zk}\Delta z_k$, provided Δz_k is sufficiently small;

TABLE III
UNIT COMMITMENT PATTERN FOR ANALYSIS II (IN MW OR MVAR)

Tie line bus	π_p	π_q
6	-0.0816	-0.1589
7	-0.9846	-1.4436
8	-0.5999	-0.9711
13	-0.0036	-0.0004
23	-0.0003	0.0001

TABLE IV
SHADOW PRICES FOR TIE LINE FLOWS

c	10	100	1000	10000
iter	21	17	17	26

when z_k hits the lower bound, as z_k min increases Δz_k , the total load will decrease $\pi_{zk}\Delta z_k$, provided Δz_k is sufficiently small. Similar comments can be applied to π_{ri} .

For example, for the unit commitment shown in Table I, when we calculate minimum load curtailment by assuming 4 zones as described before, we have $\pi_D = [-0.9294, 0, -0.0002, 4.1260]$. Since $\pi_{D1} < 0$ and has large magnitude, we expect $P_{D\Sigma 1}$ to hit the upper limit of 957.3 MW. Since $\pi_{D4} > 0$ and has large magnitude, we expect $P_{D\Sigma 4}$ to hit the lower limit 0. These expectations are verified by our calculation. Furthermore, if we raise $P_{D\Sigma 1 \max}$ by 500 MW, then $P_{D\Sigma} = [1457.3, 204.2, 106.3, 0.1]$ MW, the total load becomes 1767.8 MW, 458.3 MW more than the original one. However, if we raise $P_{D\Sigma 2 \max}$ to be 500 MW more, $P_{D\Sigma} = [957.3, 219.3, 132.9, 0]$ MW, the total load is 1390.5 MW, almost unchanged compared with the original result. Therefore, the shadow prices are useful in identifying the most effective means of improving the objective. Similar comments can be applied to π_{pk} , π_{qk} and π_{vk} . We can even use shadow prices for rough economic analysis in the planning stage.

B. "Shadow Prices" for Tie Line Flow

When there is a constant P_{Dk}^0 , π_{pk} can also be explained as the shadow price of P_{Dk}^0 . In order to illustrate this, we change our unit commitment to be as shown in Table III. Assume the total required load is $0.95 \times \text{total generation}$, and assign loads proportionally in zones, that is, $P_{D\Sigma \max} = [1571.1, 931.5, 306.4, 140.8]$ MW. Now change the swing bus from bus 23 to bus 13. Our calculation result is $P_{D\Sigma} = [1571.1, 931.5, 285.0, 140.7]$ MW. The total load curtailment is 21.4 MW. Suppose there are tie lines connected between buses 6, 7, 8, 13, 23 and the outer power systems respectively. Table IV shows the shadow prices for tie lines.

If the price for MW or MVAR input at each tie line bus is the same, we should buy MVAR power from the tie line at bus 7, because it is the most valuable power (shadow price -1.4436 , the negative sign means increasing the input tie line flow will increase the ML). Now increase Q_{D7}^0 to 10 MVAR and recalculate. We get $P_{D\Sigma} = [1571.1, 931.5, 299.1, 140.7]$ MW, the

total load curtailment is 7.3 MW, 14.1 MW less than the original case. However, if we buy active power 10 MW from bus 23's tie line, $P_{D\Sigma} = [1571.1, 931.5, 285.0, 140.7]$ MW, the total load curtailment is 21.4 MW, almost unchanged compared with the original one.

VIII. CONCLUSION

The direct interior point algorithm can be applied in power system maximum loadability calculation. The model based on the first order KT condition is simplified in this paper. Equations for generalized zone-based maximum loadability problem are derived. The maximum loadability as well as the minimum load curtailment is calculated for various conditions. The meaning of shadow prices are explained and the influence of the tie line flow is investigated. The ATC calculations with and without the thermal overload constraints are discussed. The principle of oscillation and the factors that affects the algorithm's speed and convergence are explained and investigated. Our program is first employed to calculate voltage stability bifurcation point and compared with a standard continuation power flow program VSTAB. The fact that the two results coincide with each other verifies our program. Then our proposed technique is shown to be able to handle various maximum loadability problems due to different constraints in a multi-zone system. Moreover, "shadow prices" are shown to be efficient in identifying the most effective means of increasing the maximum loadability. Our research proves the interior point algorithm is a powerful tool which can handle various kinds of maximum loadability problems, and there exist several techniques to enhance the algorithm's speed and convergence.

ACKNOWLEDGMENT

The authors would like to acknowledge the valuable suggestions of Dr. Z.-h. Feng, Ph.D. students W. Fu, and H. Wan.

REFERENCES

- [1] V. Ajjarapu and C. Christy, "The continuation power flow: A tool for steady state voltage stability analysis," *IEEE Trans.*, vol. PWRS-6, no. 2, pp. 145–156, February 1991.
- [2] N. Yorino, S. Harada, and H. Chen, "A method to approximate a closest loadability limit using multiple load flow solutions," in *IEEE PES Winter Power Meeting*, 96 WM 309-5-PWRS.
- [3] T. J. Overbye, "A power flow measure for unsolvable cases," in *IEEE PES Summer Meeting*, 93 SM 492-9 PWRS.
- [4] I. Kurihara, K. Takahashi, and B. Kermanshahi, "A new method of evaluating system margin under various system constraints," in *IEEE PES Winter Power Meeting*, 95 WM 161-0 PWRS.
- [5] G. L. Torres and V. H. Quintana, "Optimal power flow via interior point methods: An educational tool in matlab," in *Canadian Conference on Electrical and Computer Engineering, CCECE'96*, May 1996.

- [6] A. C. G. Melo, J. C. O. Mello, and S. Granville, "The effects of voltage collapse problems in the reliability evaluation of composite systems," in *IEEE PES Winter Power Meeting*, 96 WM 316-0 PWRS.
- [7] S. Granville, J. C. O. Mello, and A. C. G. Melo, "Application of interior point methods to power flow unsolvability," *IEEE Trans. on Power Systems*, vol. 11, no. 2, May 1996.
- [8] W. Wan, G. C. Ejebe, J. Tong, and J. G. Waight, "Preventive/corrective control for voltage stability using direct interior point method," *IEEE PICA*, 1997.
- [9] G. D. Irisarri, X. Wang, J. Tong, and S. Mokhtari, "Maximum loadability of power systems using optimization method," in *IEEE PES Winter Power Meeting*, 96 WM 207-1-PWRS.
- [10] K. R. Frisch, *The Logarithmic Potential Method for Convex Programming*. Norway: Institute of Economics, University of Oslo, May 1955.
- [11] N. Karmarkar, "A new polynomial-time algorithm for linear programming," *Combinatorica*, vol. 4, pp. 373–395, 1984.
- [12] S. Mehrotra, "On the implementation of a (primal–dual) interior point method," *SIAM Journal on Optimization*, vol. 2, no. 4, pp. 575–601, 1992.
- [13] Y. Y. Ye, *Interior Point Algorithms: Theory and Analysis*. New York, NY: Wiley, c1997.
- [14] B. Jansen, *Interior Point Techniques in Optimization: Complementarity, Sensitivity, and Algorithms*. Dordrecht/Boston: Kluwer Academic, c1997.
- [15] X. Yan and V. H. Quintana, "Infeasible interior point algorithm for optimal power flow problems," *Electric Power Systems Research*, vol. 39, no. 1, Oct. 1996.
- [16] M. Christoforidis, M. Aganagic, B. Awobamize, S. Tong, and A. F. Rahimi, "Long-term/mid-term resource optimization of a hydro-dominant power system using interior point method," *IEEE Trans. on Power Systems*, vol. 11, no. 1, pp. 287–294, Feb. 1996.
- [17] Powertech Labs Inc., "Release Notes for VSTAB Version 4.1.," Surrey, BC, Canada, Jan. 1996.
- [18] "The reliability test system task force of the application of probability methods subcommittee," in *The IEEE Reliability Test System-1996*, 96 WM 326-9 PWRS.

Youjie Dai was born in Chengdu, China. He received his B.E. degree from Xi'an Jiaotong University in 1992, and M.E. degree from Tsing Hua University in 1995, both in electrical engineering. He is currently working toward his Ph.D. in electrical engineering at Iowa State University. His research interests include stochastic load model identification and application, risk assessment in the new deregulated power system, and Monte Carlo simulation. He is now a Student Member of IEEE.

James D. McCalley is an Associate Professor of Electrical and Computer Engineering Department at Iowa State University, where he has been employed since 1992. He worked for Pacific Gas and Electric Company from 1986 to 1990. Dr. McCalley received the B.S. (1982), M.S. (1986), and Ph.D. (1992) degrees in electrical engineering from Georgia Tech. He is a registered Professional Engineer in California and a Senior Member of the IEEE.

Vijay Vittal is Professor of the Electrical and Computer Engineering Department at Iowa State University. He received the B.E. (1977) in electrical engineering from Bangalore, India, the M.Tech. (1979) from the Indian Institute of Technology, Kanpur, India, and the Ph.D. (1982) from Iowa State University, Ames, Iowa. He is the recipient of the 1985 Presidential Young Investigator Award. He is a Fellow of the IEEE.